THE ASTRONOMICAL JOURNAL, 117:2841–2855, 1999 June

STATISTICS OF STELLAR POPULATIONS OF STAR CLUSTERS AND SURROUNDING FIELDS IN THE OUTER DISK OF THE LARGE MAGELLANIC CLOUD

JOÃO F. C. SANTOS, JR.
Departamento de Física, ICEx, Universidade Federal de Minas Gerais, CP 702, 30123-970 Belo Horizonte MG, Brazil
ANDRÉS E. PIATTI[1] AND JUAN J. CLARIÁ[1]
Observatorio Astronómico de Córdoba, Laprida 854, 5000, Córdoba, Argentina
EDUARDO BICA
Departamento de Astronomia, Instituto de Física, Universidade Federal do Rio Grande do Sul, CP 15051, 91501-970 Porto Alegre RS, Brazil
DOUG GEISLER
Departamento de Física, Universidad de Concepción, Casilla 160-C, Concepción, Chile; doug@stars.cfm.udec.cl
AND
HORACIO DOTTORI
Departamento de Astronomia, Instituto de Física, Universidade Federal do Rio Grande do Sul, CP 15051, 91501-970 Porto Alegre RS, Brazil
Received 1999 February 11; accepted 1999 March 10

ABSTRACT

A comparative analysis of Washington color-magnitude diagrams (CMDs) for 14 star clusters and respective surrounding fields in the Large Magellanic Cloud (LMC) outer disk is presented. Each CCD frame including field and the respective cluster covers an area of 185 arcmin^2. The stellar population sampled is of intermediate age and metallicity. CMD radial analysis involving star count ratios, morphologies, and integrated light properties are carried out. Luminosity functions (LFs) are also presented. The two main results are, (1) within the range 4 kpc $< R <$ 8 kpc, the distance from the LMC center is well correlated with the average age in the sense that inner fields are younger and (2) beyond $\approx$8 kpc the outer fields do not show evidence of a significant intermediate-age component in their stellar populations, as inferred from red giant clump star counts.

Key words: galaxies: star clusters — galaxies: stellar content — Magellanic Clouds

1. INTRODUCTION

The stellar populations making up galaxies mix and change as a result of dynamical processes and stellar evolution. Star clusters can probe the galaxy's history, as they represent a unique population born in a star formation burst. Field stars, as opposed to cluster stars, do not constitute gravitationally bound systems and reflect a mix of stellar populations whose local nature is revealed more efficiently through individual star photometry, i.e., through color-magnitude diagrams (CMDs). In spite of the recent advances in telescope and detector technologies, just a handful of galaxies can be investigated through this technique, foremost among them being the Magellanic Clouds. Galaxies beyond the Local Group are not yet reachable at magnitude levels useful for a statistical treatment of their field stellar populations by using individual star photometry.

Studies of the intermediate-age stellar populations of LMC fields were reviewed by Olszewski, Suntzeff, & Mateo (1996) and summarized in their Table 2. The only study sampling field sizes larger than in present work is the photographic one by Stryker (1984), but the size of the population observed is much smaller. (Note that their Table 2 shows the Hodge 1987 observations as sampling an area of 400 arcmin^2 although the correct area is 20 arcmin^2). Stryker, by observing fields lying 9 kpc from the LMC bar, suggested that a major portion of the stellar content of the LMC is of intermediate age.

Similarly, Butcher (1977), Hardy et al. (1984), Bertelli et al. (1992), Westerlund, Linde, & Lingå (1995), and Vallenari et al. (1996), among others, observed and analyzed CMDs of field populations in the LMC bar and disk. The results obtained from their ground-based observations agree and indicate a global burst of star formation to have occurred in the LMC $\approx$3–4 Gyr ago.

In particular, Bertelli et al. (1992) observed three fields in the LMC located at distances less than 6° from the LMC center. Their CCD frames cover 15 arcmin^2. They computed ratios of star counts in the CMDs of fields near the clusters NGC 1783, NGC 1866, and NGC 2155 in order to investigate the star formation history of the LMC. Synthetic CMDs were built by using stellar evolutionary models and assuming an initial mass function coupled to a star formation rate described by the relative strength of the burst and the ages of the beginning and end of the burst. Their analyses show that a Salpeter initial mass function (IMF) slope is plausible for all fields, and all are characterized by having a burst beginning at a similar age, i.e., 3–4 Gyr ago. After this burst began, the mean star formation rate in the LMC has been increased 10 times up to at least 1 Gyr ago at places as far as $\approx$5 kpc from the LMC center. The star formation in the central regions of the LMC is continuing to the present day.

Observing smaller fields, Westerlund et al. (1995) obtained different results for two fields $\approx$6° apart lying at distances $\approx$4.5° from the LMC center. Their northwest field has a dominant stellar component younger (0.3–0.8 Gyr) than that making up their southwest field. Not only fields, but also clusters follow this trend. Both fields contain a well-represented intermediate-age population (1–3 Gyr),

[1] Visiting Astronomer, Cerro Tololo Inter-American Observatory, which is operated by AURA, Inc., under cooperative agreement with the NSF.

which led the authors to infer that a global star formation burst occurred ≈ 3 Gyr ago.

Hubble Space Telescope (*HST*) observations, although sampling smaller area fields, produce deeper photometry than ground-based observations. Geha et al. (1998), and references therein, have investigated three LMC fields at 3°–4° from the bar center, one located to the northeast and two to the northwest. They suggested that there has been more star formation in the past than was previously believed. Their models, assuming a standard IMF slope, indicate that the star formation rate was nearly constant for 10 Gyr, then it increased by a factor of 3 for the last 2 Gyr. On the other hand, Elson, Gilmore, & Santiago (1997) show evidence for a major star-forming event to have occurred ≈ 2 Gyr ago, in agreement with ground-based studies.

The studies of LMC intermediate-age star clusters were also reviewed by Olszewski et al. (1996). Data for those clusters that have CMDs not severely affected by field contamination were summarized by Geisler et al. (1997). Besides the clusters listed by Geisler et al. (1997), NGC 1987 and NGC 2108 were also observed in *UBV* by Corsi et al. (1994), and NGC 1806 has been observed in *JHK*, but the resulting CMD contains only giant stars (Ferraro et al. 1995). It is well known that the LMC cluster distribution presents a lack of clusters between ≈ 3 Gyr and ≈ 12 Gyr, the one exception being ESO 121-SC03, with an age of ≈ 9 Gyr. In a recent study using the *HST*, Sarajedini (1998) obtained ≈ 4 Gyr for the age of three populous clusters (NGC 2155, SL 663, and NGC 2121), claiming not only that those clusters fill the age gap if the adopted metallicity is [Fe/H] $= -1.0$, but also acknowledging the need for a larger sample of intermediate-age clusters in order to constrain the LMC cluster-formation history in this age range.

All of these investigations involve analyses of stellar evolutionary phases recognizable from their location in the CMD, as well as studies of luminosity functions. Ratios of star numbers in CMDs were also employed in some cases.

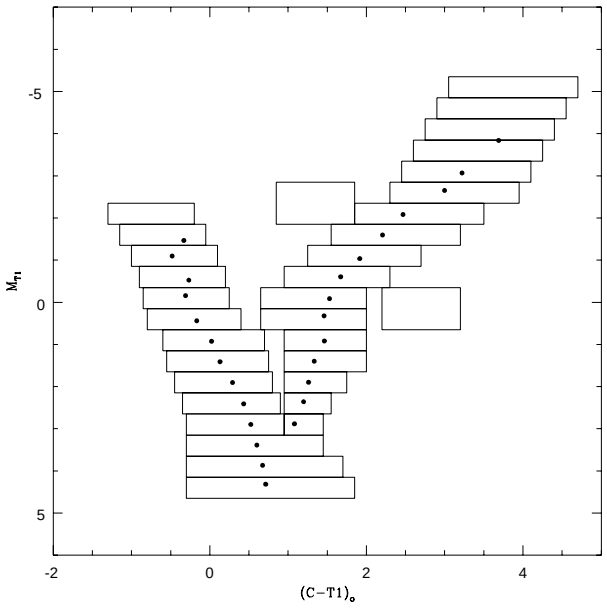

FIG. 1.—31 CMD boxes enclosing the main evolutionary sequences presented by intermediate-age stellar populations plus the two boxes used for measuring the Galactic contamination (*empty wider boxes*). Dots mark the flux averaged T_1 magnitude and mean color of the stars, within each box, for an annular field surrounding SL 769 (500 pixels $< r <$ 691 pixels).

In a recent work, Geisler et al. (1997) employed the Washington system (Canterna 1976) in a search for old LMC star clusters and narrowed down the uncertainties on the cluster-formation history of the LMC for ages greater than ≈ 1 Gyr. More recently, Bica et al. (1998) used the same database to determine that most of their sample of clusters and fields, which belong to the LMC outer disk (distance > 4 kpc from the LMC bar center), are of intermediate age (1 Gyr $\leq t \leq 3$ Gyr) and metallicity ($-1.1 \leq$ [Fe/H] ≤ -0.4). Exceptions are ESO 121-SC03 ($t \approx 9$ Gyr) and SL 769 (an inner-disk cluster).

This paper presents the third in our series based on the Geisler et al. (1997) data. The present study involves an analysis of a sample of Washington CMDs of clusters and populous fields located in the LMC disk, using star counts as a valuable source of information regarding stellar population variations throughout that galaxy. A comparison of cluster and spatially related field stars is another goal that can be accomplished through star counts. In some cases, proceeding with such analysis involves considering poor statistics, crowded fields, and Galactic star contamination, among other effects such as differential reddening across the LMC. In order to count stars in different phases of evolution, a set of boxes limiting regions in the CMD was employed, making it possible to determine luminosity functions and to evaluate Galactic star contamination.

Several factors make the present work an improvement on previous studies; the larger field sizes and the variety of positions and larger distances from the LMC center. Large fields yield better statistics for CMD based studies, such as the radial behavior of star counts in different evolutionary stages. Fields spread out in distance give an opportunity to analyze radial gradients of stellar population parameters.

The sample is presented in § 2. The procedure employed to count stars in the CMDs is described in § 3, where also the contamination by Galactic stars is accounted for and luminosity functions of cluster and fields are presented. Discussions of the morphology of field CMDs, radial properties of the sample, and ratios of star counts are given in § 4. Finally, § 5 outlines the conclusions, and an Appendix giving an analysis of crowding is also included.

2. THE DATA

The observations are detailed in Geisler et al. (1997) and Bica et al. (1998). In summary, the observations were carried out with the Cerro Tololo Inter-American Observatory (CTIO) 0.9 m telescope with the Tek2k No. 3 CCD. The scale on the chip is 0.″40 pixel^{-1}, yielding an area of 13.′6 $\times$ 13.′6. SL 769 was observed with the CTIO 4 m with the Tek2k No. 4 CCD, with similar pixel and areal coverage. The filters used for both runs were the Washington *C* and Kron-Cousins *R* filters and the observations were calibrated in the *C*, T_1 Washington system. The data were reduced with DAOPHOT II (Stetson 1987) after trimming, bias subtraction, and flat fielding. Typically 10% of the detected objects in a frame were discarded as a result of adopting criteria aiming at reducing errors. More details on the observations, reductions, and calibration procedures were given in Geisler et al. (1997).

TABLE 1

CLUSTERS AND SURROUNDING FIELDS

Cluster ID (1)	α_{1950} (2)	δ_{1950} (3)	I (deg) (4)	b (deg) (5)	N (6)	r (deg) (7)	R (deg) (8)	$E(C-T_1)$ (9)	(T_1-M_{T1}) (10)	Age (Gyr) (11)	[Fe/H] (12)
SL 8, LW 13	04 38 00	−69 07 37	280	−38.2	75	3.9	5.5	0.08	18.60	1.8:	−0.50
Field					4355					2.0	−0.35
SL 126, ESO 85-SC21	04 56 53	−62 36 37	272.5	−36.9	101	7.5	8.0	0.02	18.53	2.2	−0.45:
Field					1437					>2.5	−0.45
SL 262, LW 146	05 08 52	−62 26 27	272.0	−36.0	104	7.2	7.4	0.00	18.50	2.1	−0.55
Field					1737					2.0	−0.50
SL 388, LW 186	05 19 44	−63 31 44	273.1	−34.2	200	6.0	6.0	0.06	18.58	2.2	−0.65
Field					6421					2.0	−0.60
IC 2134, SL 437, LW 198[a]	05 24 47	−75 29 26	287.1	−31.7	119	6.0	6.0	0.20	18.76	1.0	...
Field					4885					2.0	−0.70
SL 451, LW 206[a]	05 25 57	−75 36 33	286	−31.6	68	6.1	6.1	0.20	18.76	2.2	−0.70:
Field					4885					2.0	...
SL 509, LW 221	05 29 29	−63 41 11	273.2	−33.1	217	5.9	6.0	0.06	18.58	1.2	−0.85
Field					10131					1.5	−0.50
SL 769[b]	05 53 54	−70 04 44	281	−30.3	203	2.8	4.0	0.16	18.71	1.8	−0.45
Field					57222					...	−0.50
SL 817	06 01 09	−70 04 07	280	−29.7	66	3.4	4.8	0.14	18.68	1.5	−0.50:
Field					10142					2.0	−0.70
ESO 121-SC03[c]	06 01 27	−60 31 17	269.5	−29.4	394	10.3	11.4	0.06	18.58	8.5	−1.05
Field					441					9.0	...
SL 842, LW 399	06 07 53	−62 58 40	272.3	−28.8	57	8.4	9.9	0.06	18.58	2.2	−0.60
Field					1591					2.5	−0.55
SL 862, LW 431	06 14 04	−70 40 45	281.1	−28.6	110	4.5	6.3	0.18	18.74	1.8	−0.85
Field					4772					2.0	−0.60
OHSC 33	06 16 33	−73 45 58	284	−28.5	47	5.7	6.9	0.18	18.74	1.4	−1.00
Field					4022					2.0	−0.65
OHSC 37	07 08 01	−69 54 10	280	−24.0	27	9.2	13.0	0.29	18.89	2.1	−0.65
Field					559					...	...

NOTE.—Ages, metallicities, and photometric indexes are from Bica et al. 1998. Units of right ascension are hours, minutes, and seconds, and units of declination are degrees, arcminutes, and arcseconds.

[a] IC 2134 and SL 451 are located in the same frame.

[b] SL 769 is an inner disk cluster.

[c] ESO 121-SC03 is the oldest cluster in the sample (8.5 Gyr).

The clusters and fields sample is presented in Table 1. Clusters have the following catalog designations: SL (Shapley & Lindsay 1963), LW (Lyngå & Westerlund 1963), ESO (Lauberts 1982), and OHSC (Olszewski et al. 1988). Column (1): Cluster identification with respective surrounding field; columns (2) and (3): equatorial coordinates; columns (4) and (5): Galactic coordinates; column (6): number of stars sampled; column (7): distance in degrees from the LMC center, adopted as the position of the cluster NGC 1928, $\alpha_{1950} = 5^h21^m19^s$ and $\delta_{1950} = -69°31'30''$; column (8): deprojected distance in degrees from the LMC center assuming all clusters within the outer disk tilted at $i \sim 45°$; columns (9) and (10): reddening and distance moduli according to the relations $E(C-T_1) = 1.966E(B-V)$, $A(T_1) = 2.62E(B-V)$, and $(m-M)_o = 18.5$; and columns (11) and (12): age and metallicity according to determinations in Bica et al. (1998).

Relationships between the Washington and UBV systems adopted here are those by Geisler (1996). Namely, two useful equations are $V = 0.052 + T_1 + 0.256(C-T_1)$ and $B-V = 0.076 + 0.475(C-T_1)$.

Except for ESO 121-SC03 (an old cluster) and SL 769 (an inner disk cluster), the sample of clusters and surrounding fields have intermediate ages and belong to the LMC outer disk. Their metallicities are in the range $-1.05 \leq$ [Fe/H] ≤ -0.35.

3. STAR COUNT ANALYSIS

In the following a detailed description of the procedure adopted to study the LMC stellar population sampled in the CMDs is presented.

3.1. *Box Definitions*

By sorting out stars in boxes encompassing fundamental bright evolutionary sequences in the CMD, it is possible to count them and to study absolute numbers and their ratios. This is especially useful for the fields we have, where crowding is not serious and where areal extractions in the frames throughout the LMC are comparable. Boxes were defined in the CMDs enclosing 14 regions on the main sequence (MS) and 17 regions from the subgiant branch (SGB) to the giant branch (GB) tip, passing by the red giant clump (RGC). Another two boxes account for Galactic contamination. In Figure 1 the boxes are shown together with color and magnitude averages of stars within an annular area (500 pixels $< r <$ 691 pixels) of the field around SL 769.

Luminosity functions (LFs) were derived for the MS and the GB with a 0.5 mag bin in T_1 (the boxes' width). The field CMD of SL 769 (youngest in the sample) was used in order to define the boxes' length ($C-T_1$ color range) as well as their position in the diagram. Such positions were chosen

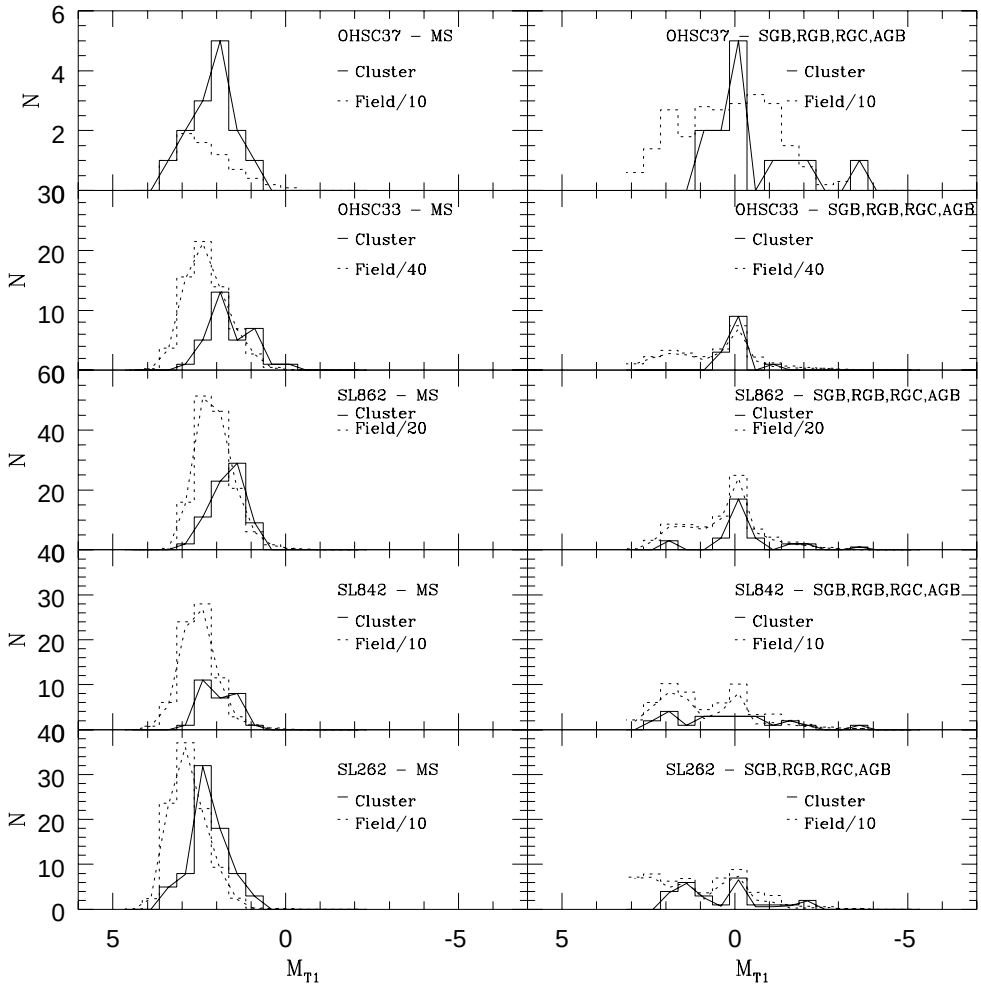

FIG. 2*a*

FIG. 2.—(*a*) Histogram of the luminosity function for cluster and respective fields separated into (*left panel*) the MS LF and (*right panel*) the GB LF. Solid lines represent cluster LFs and dashed lines field LFs. LFs corrected for Galactic contamination are shown as continuous curves. The field shown in the upper panel is the one used as a sample of the Galactic field. (*b*) Same as (*a*) for different clusters and fields. (*c*) Same as (*a*) for the most populous fields.

with the aim of at enclosing stars in the main evolutionary sequences. Since the field surrounding SL 769 contains the youngest population of our sample, the remaining clusters and fields do not populate boxes in the upper MS. LFs for all the sample were built with the complete set of boxes, independently of the population age, for the sake of uniformity. Some clusters have relatively small numbers of stars (see Table 1) and little information can be extracted from their LFs. On the other hand, most of the fields are populous, and their LFs are statistically meaningful.

Star counts within these boxes were performed, allowing a comparison between the cluster and respective field populations. In order to get reliable luminosity functions the effect of Galactic foreground stars on the star counts was taken into account. Crowding was also considered. In the Appendix a theoretical approach to evaluate crowding is used and compared to the present photometric data. No corrections for incompleteness and differential reddening were applied (the latter effect should be negligible in all of these outer disk fields).

3.2. *Accounting for Galactic Star Contamination*

The extent of field contamination of each cluster CMD was checked in Bica et al. (1998) by obtaining an equal-area field CMD composed of the addition of CMDs derived from four different fields, each with an area 1/4 that of the cluster and lying far away from the cluster. Such a comparison was an overestimate for the field contamination since the photometric limit within the cluster is brighter than in the field, and more stars are discarded from the cluster because of larger photometric errors due to increased crowding. Nevertheless, in only one outlying cluster was the number of stars obtained in the equal-area field significantly higher than 1/4 of the stars in the cluster CMD. The typical ratio was only $\sim 10\%$. Here a different approach was used to evaluate field contamination by foreground Galactic stars on the cluster and field CMDs.

The CMD of the field surrounding OHSC 37, the outermost cluster in our database, was used as a sample of Galactic field contamination, since Bica et al. (1998) found no indications of any LMC field stars there. The Galactic contamination was accounted for in the LMC clusters and fields by using two control boxes in the CMDs gauging the number of stars in loci clearly off the main evolutionary sequences. In the field surrounding OHSC 37, the ratio of star counts within these two Galactic field boxes and the LMC cluster or field boxes gives the correction factor used to infer the relative number of Galactic field stars on the

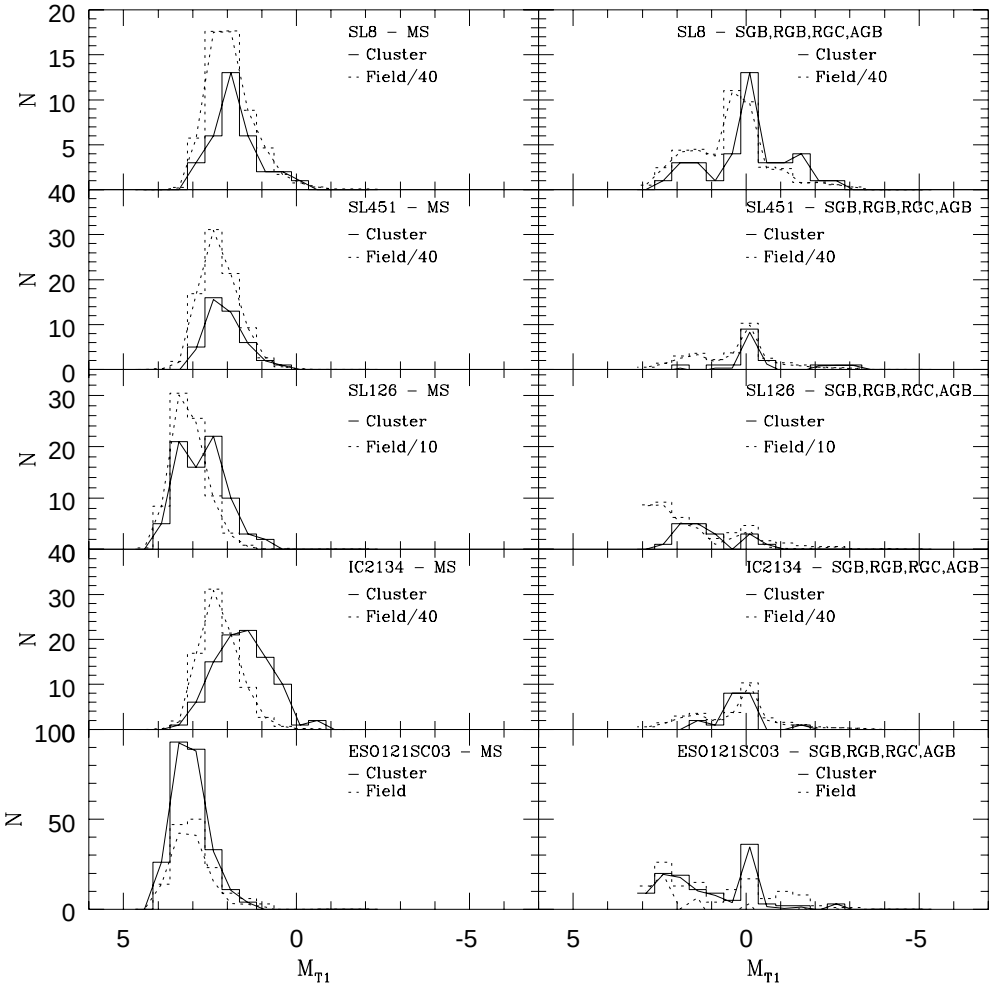

FIG. 2*b*

CMD sample. Since some boxes in the field surrounding OHSC 37 have only a small number of stars, it would be best to check such a correction by using more detailed studies.

Ratnatunga & Bahcall (1985, hereafter RB85) estimated the contribution of Galactic field stars in various directions including one toward the LMC. In that direction, considering $E(B-V) = 0.06$, the star density predicted by the Galaxy models of Bahcall & Soneira (1980, hereafter BS80) in the photometric box $0.8 < B-V < 1.3$ and $17 < V < 19$ is 0.16 arcmin^{-2}. At a fainter bin, $19 < V < 21$, and the same color range, the star density is 0.13 arcmin^{-2}. In order to compare these values with our Galactic field sample (the field surrounding OHSC 37), it is advisable to note that OHSC 37 is far from the LMC center, 9° closer to the Galactic equator, and has a higher reddening value $[E(B-V) = 0.15]$. Both factors suggest an increase in star density. To measure the star density in the observed field, calibrations relating Washington and Johnson photometry were employed (Geisler 1996) to transform our observed $T_1 \times (C-T_1)$ CMD into a $V \times (B-V)$ one. After performing these transformations, star counts in the CMD of the field surrounding OHSC 37 in the same photometric windows resulted in star densities of 0.43 arcmin^{-2} and 0.4 arcmin^{-2}, respectively, which are significantly larger than the values given by the model, as expected. A comparison of model star densities at different positions and reddenings led us to conclude that the discrepancy between the CMD counts and the RB85 predictions is mainly produced by differences in Galactic latitude.

The CMD for the field surrounding OHSC 37 contains 559 stars, which makes it a statistically good estimator for Galactic contamination toward that direction. The whole sample, however, spreads over distances of $\approx 10°$ around the LMC center; therefore, variations of the Galactic foreground star density are expected among the LMC regions analyzed in the present work. There follows a more precise attempt to see how large such a variation is and how comparable modeled and observed star densities toward OHSC 37 are.

Given the Galactic latitude (b) and longitude (l) as well as a V magnitude, the Galaxy models of BS80 compute cumulative star counts (for magnitudes brighter than V) toward the indicated direction and allow one to redden the models in order to directly compare them with the observations. Table 2 compares star densities in our observed sample of the Galactic field with the one predicted by BS80. For each 2 mag bin investigated the observed star density is slightly smaller than the one predicted by the models, taking into account the star density errors quoted by BS80 (25%). It should be noticed that the $V = 22 \pm 1$ bin does not contain a statistically complete star sample since there are essentially no stars fainter than $T_1 = 22.5$ ($V \approx 22.8$) in the analyzed photometry.

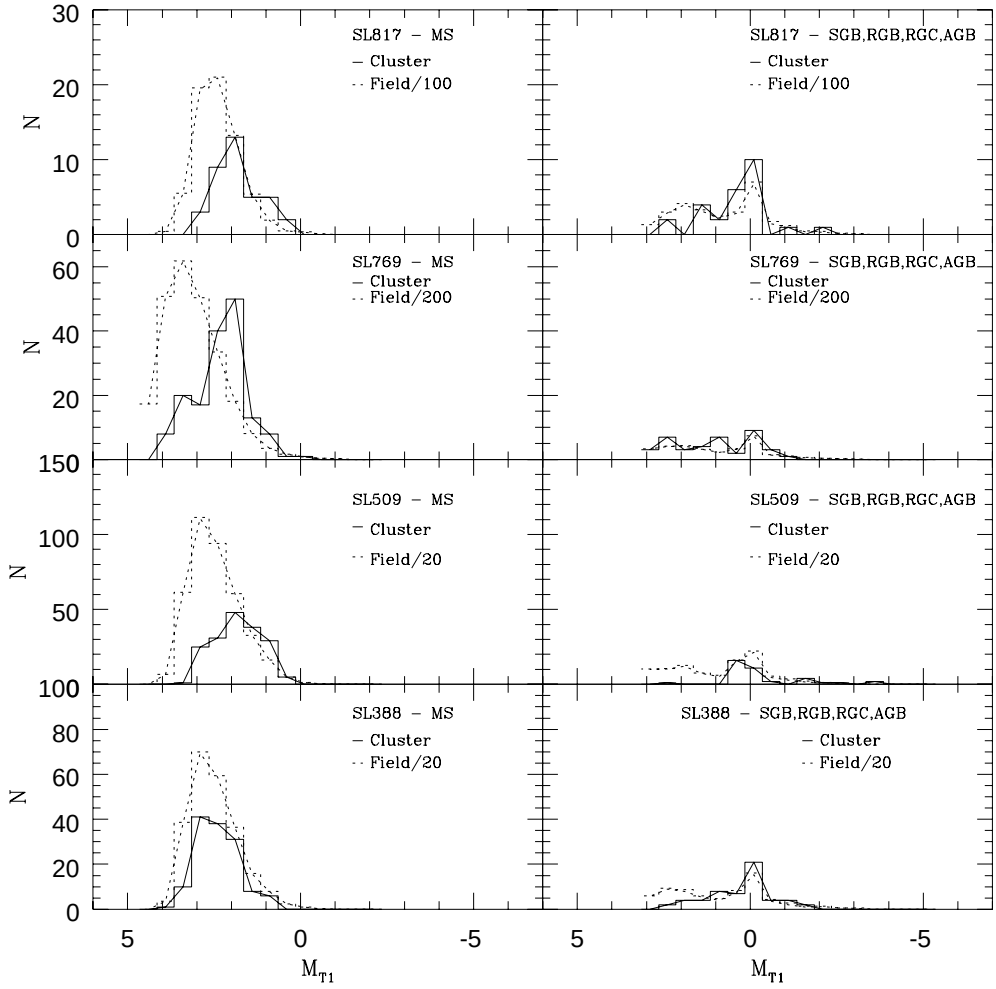

FIG. 2*c*

The field taken as representative of Galactic contamination should sample the highest number of foreground stars when compared to the remaining fields because it is closest to the Galactic plane. Thus, the correction factor derived from it should be taken as an upper limit when applied to the other fields. On the other hand, Table 2 shows that the star densities used to derive this correction factor are slightly below those determined theoretically. The boxes in the CMDs enclosing the main evolutionary sequences and nearby regions are a preliminary way to get rid of stars clearly pertaining to the Galaxy. An estimate of the density of Galactic field stars within the CMD boxes was made to get more reliable LFs. Specifically, the pro-

TABLE 2

STAR DENSITIES (N arcmin^{-2})

V Bin (± 1)	OHSC 37 Field	BS80 Model
14.....	0.05 (10)	0.13 ± 0.03
16.....	0.24 (43)	0.36 ± 0.09
18.....	0.82 (149)	0.96 ± 0.24
20.....	1.30 (236)	1.87 ± 0.47
22.....	0.67 (121)	1.85 ± 0.46
Total (18 ± 5).....	3.07 (559)	5.17 ± 1.29

NOTE.—Values parenthesized are number of stars within the V bin. Last column shows errors according to BS80.

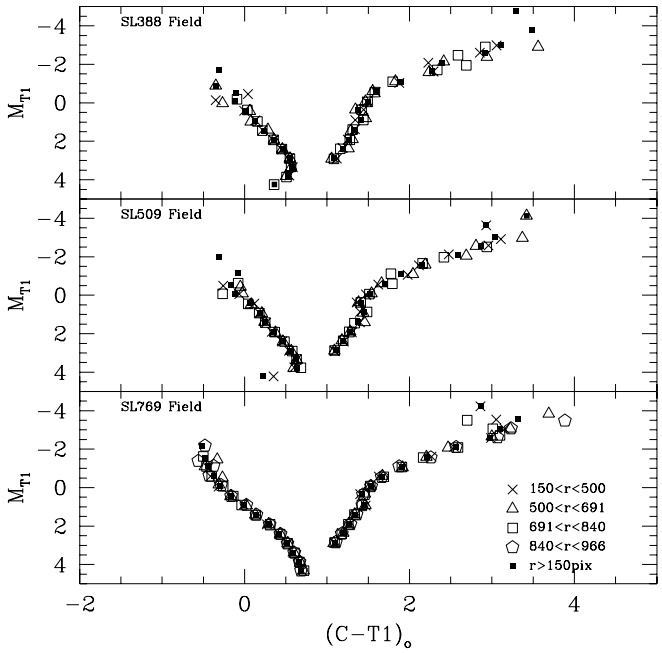

FIG. 3.—CMD mean sequences derived using the boxes for three populous fields. Each symbol defines sequences corresponding to a ring centered on the associated cluster. The filled symbol shows the mean sequence for the whole field.

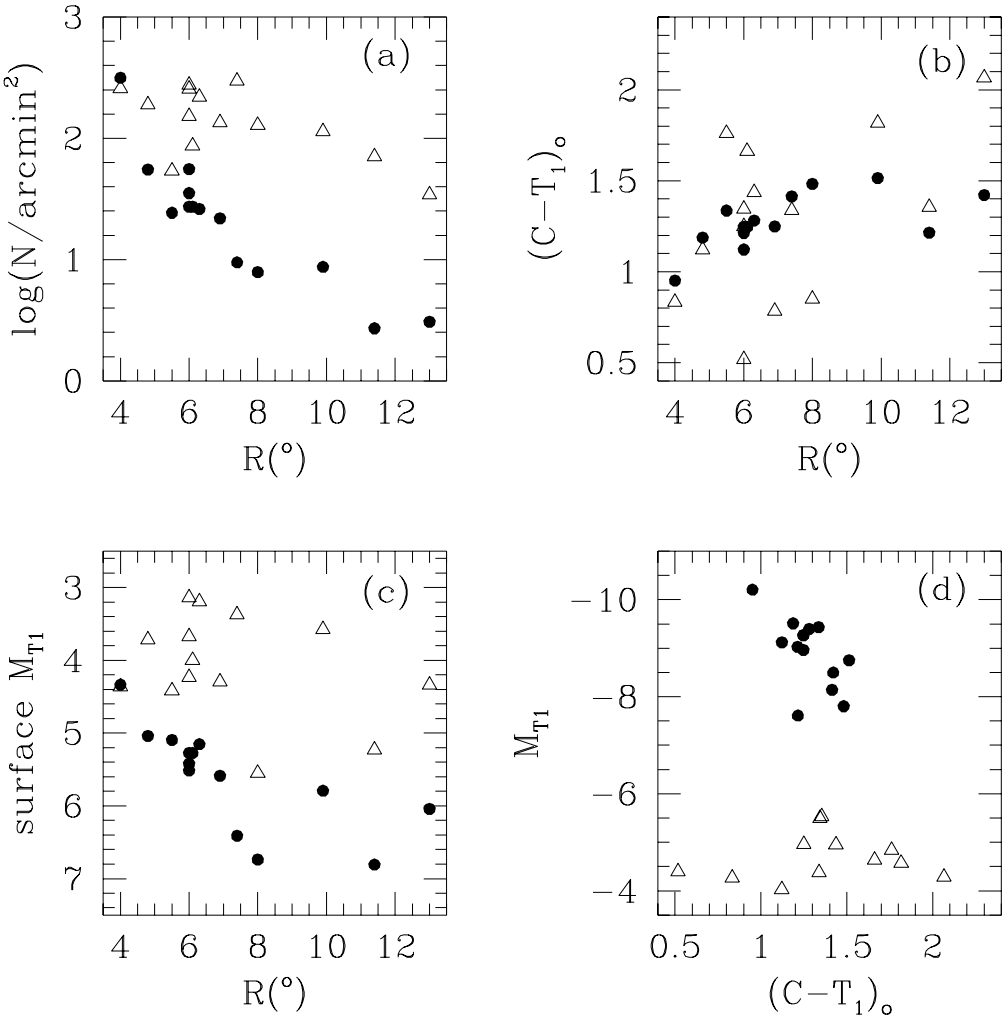

FIG. 4.—Cluster (*triangles*) and field (*filled circles*) integrated magnitudes are plotted as a function of integrated $(C-T_1)_o$. All integrated indexes are also shown against distance from the LMC center (see text for details).

cedure employed to determine the correction factor was (1) to count stars in two boxes clearly off the main evolutionary sequences present in the CMD of both the field surrounding OHSC 37 and the LMC cluster or field of interest; (2) to count stars in a given "LMC field" box representing the locus of an evolutionary sequence segment in OHSC 37; (3) to compute for all field and cluster CMDs the number of Galactic foreground stars expected in the "LMC field" box from the following expression:

$$N_i^{\rm LMC} = N^{\rm LMC} N_i^{\rm OHSC\ 37}/N^{\rm OHSC\ 37}\ , \qquad (1)$$

where N represents the sum of the number of stars in the two "Galactic field" boxes and N_i is the number of stars in the ith "LMC field" box; and (4) to repeat the calculation for all LMC field boxes making possible the construction of corrected LFs for each CMD.

3.3. *Luminosity Functions of Clusters and Fields*

Figure 2 presents the LFs of clusters and fields without (*histograms*) and with (*continuous curves*) the correction for Galactic foreground. The left panels are MS LFs, and the right panels are GB LFs. No strong effect on the LFs morphology is seen for any cluster or field as a consequence of the Galactic foreground. Figure 2*a* shows in the top panels the LF for the field used as a sample of the Galactic foreground. The field surrounding ESO 121-SC03 is the only one for which there are significant differences between the corrected and observed LF, as can be seen from the bottom panels of Figure 2*b*. Figure 2*c* presents the most populous fields LFs. Clusters and fields in general agree regarding the RGC location. A conspicuous old SGB ($2 < M_{T1} < 3$) and its corresponding ascending GB ($1 < M_{T1} < 2$) are visible only in the field LFs. Although a small number of stars were present in the MS of most of the clusters, three of them (SL 388, SL 509, and SL 842) seem to have shallower MS LFs as compared to the corresponding surrounding fields. Differences were found between clusters and respective fields in the MS LF peak, which could be due not only to crowding but, more likely, age effects. ESO 121-SC 03 and SL 451 are clearly clusters that have the maximum of the MS LF at the same magnitude as their respective fields.

4. DISCUSSION

4.1. *Field CMDs Morphology*

Is there a radial variation of any astrophysical property in each field considered individually? In order to answer such a question, the radial variation of the mean locus of the main evolutionary sequences in the CMDs for the more

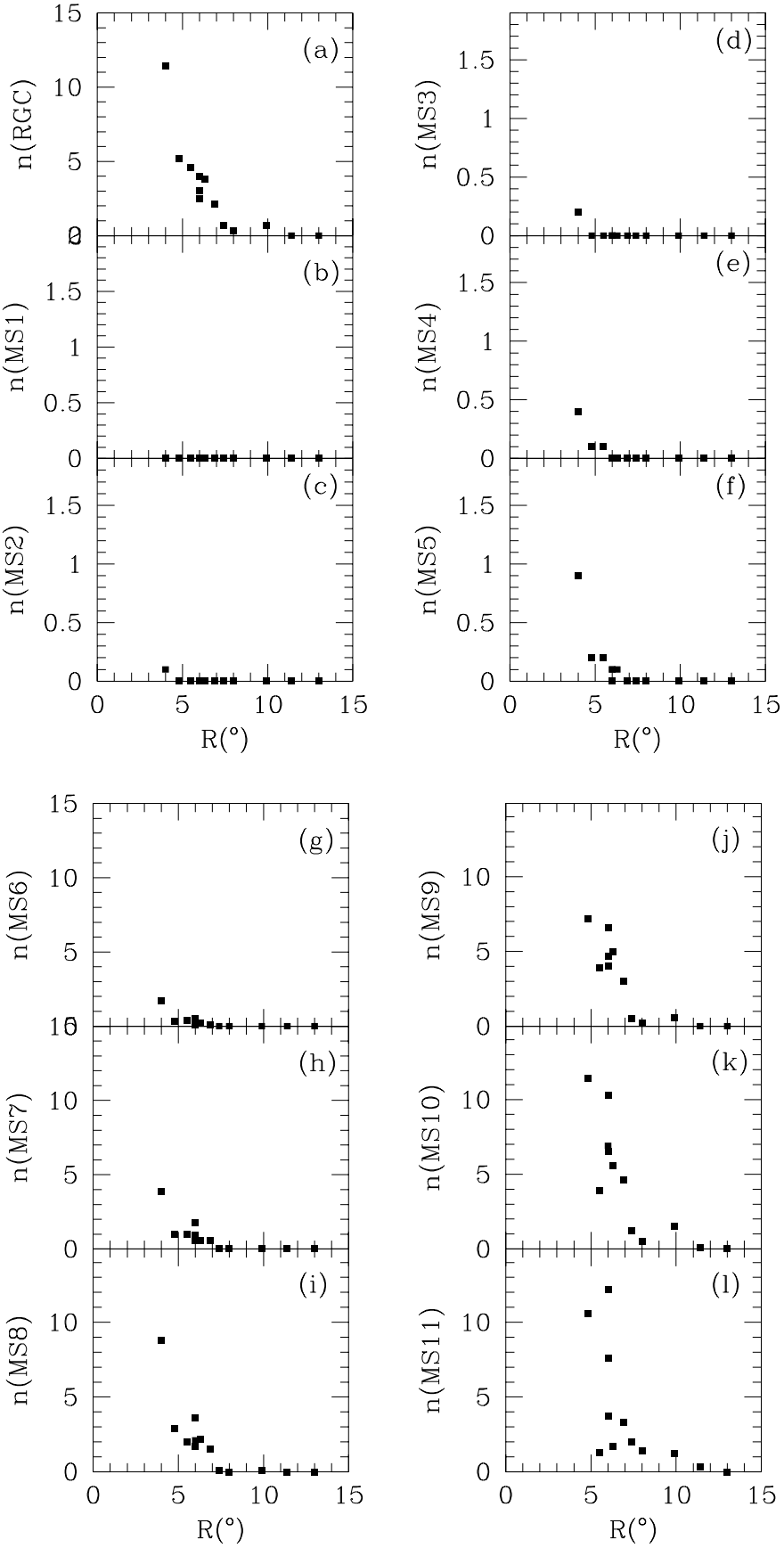

FIG. 5.—Densities of field clump stars and of stars in 11 MS CMD regions against galactocentric distance. The sequence runs from brighter (MS1) to fainter (MS11) regions.

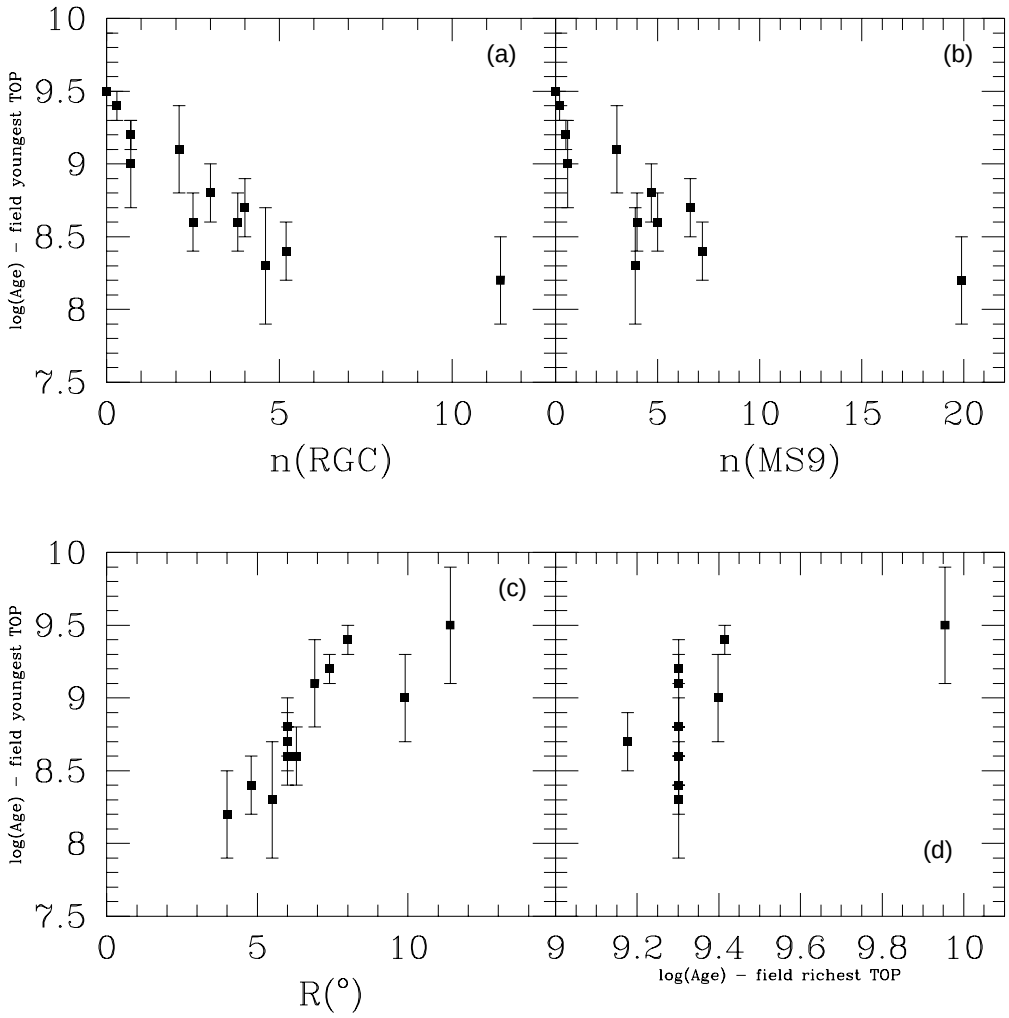

FIG. 6.—Age of the youngest stellar population in each field as a function of the (*a*) RGC stars density, (*b*) lower MS stars density, (*c*) galactocentric distance, and (*d*) age of the most populous turnoff.

populous fields was investigated. The set of boxes was used to define a mean CMD locus at different distances from the field center (coincident with the corresponding cluster center). The mean CMD locus should be understood as the position in the CMD given by the flux-averaged T_1 magnitude and the mean $C-T_1$ color of the stars within each box. Figure 3 shows the CMD sequences for four equal-area annular fields surrounding SL 769 and for three of these annular fields surrounding SL 388 and SL 509. The mean CMD sequences for the entire field ($r > 150$ pixels) are also shown. It is clear that there are no important radial changes in the CMD morphology of the four most populous fields in our sample, and, as a consequence, any possible color gradient of the central cluster no longer survives at those distances. The scatter for the brightest "mean stars" on the MS and GB is a consequence of the small number of stars in the corresponding boxes. It allows one to estimate at which magnitude the stochastic nature of the mass function becomes significant and how it depends on the size of the population. Table 3 shows the star number density, the integrated absolute M_v magnitude (as computed using the transformation relation in Geisler 1996), the integrated $(C-T_1)_o$ color, and the integrated absolute M_{T1} magnitude for each annular field and the complete one, allowing an estimate of how significant the stochastic effects are on the integrated light of those populous fields. Specifically, the spread in $(C-T_1)_o$ is 0.1 for SL 769, 0.12 for SL 509, and 0.25 for SL 388, which are in order of decreasing number of stars. By enlarging the sample of populous fields, it will be possible to better quantify these effects on purely observational grounds by means of a statistically meaningful relation between the color changes and the population size. As such, this procedure will provide constraints for stellar population studies of composite systems for which the integrated light is the only accessible observable.

4.2. *Radial Properties of the Sample*

Is there a radial variation of any astrophysical property along the LMC disk as sampled from the whole set of fields? This question was addressed by using the data in Tables 1 and 3. The density of stars in specific evolutionary phases for the fields was also analyzed as a function of distance. Ages for the youngest field population were estimated and their radial behavior investigated.

4.2.1. *Integrated Light and Density*

Figure 4 shows that the behavior of integrated properties with distance for clusters (*open triangles*) and fields (*filled circles*) is not, in general, the same. Although the poor statistics of some clusters may affect their apparent distribu-

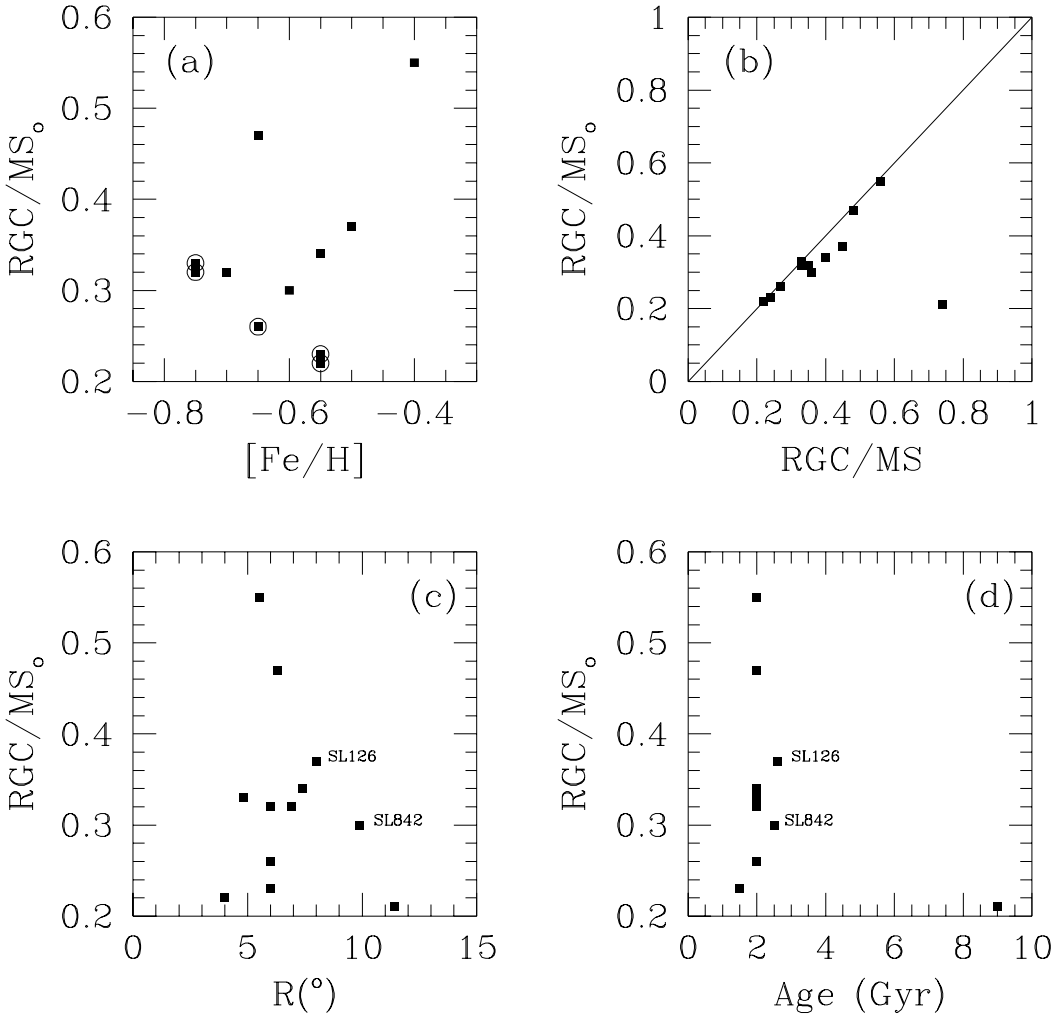

FIG. 7.—Ratio of the number of RGC stars to the number of MS stars for the fields within a bin of $\Delta M_{T1} = 0.5$, corrected for Galactic contamination, as a function of (*a*) metallicity, where the most populous fields are circled, (*b*) the uncorrected ratio, (*c*) the deprojected distance, and (*d*) age.

tion, the fields are in general sufficiently populous to make a comparative interpretation for them worth doing.

The projected stellar density of the fields decreases more abruptly toward the outer LMC regions than that of the clusters (Fig. 4*a*). A possible cause for this is suggested in the following. Both field stars and cluster stars are under the influence of the same LMC gravitational field at a given distance. Cluster stars, though, are bound because of their self-gravitation. External gravitational fields can disrupt clusters in the inner regions of the LMC. Therefore, moderately dense clusters survive, in principle, at any distance in the range 4–13 kpc from the LMC center. The slight decrease of cluster star density with distance seen in Figure 4 appears to be a consequence of a lack of low-density (less bound) clusters for the inner regions, which may have been destroyed by the tidal forces of the LMC. On the other hand, the field stars are distributed according to the LMC gravitational field, from which the steeper decrease of density as a function of distance is expected: the closer to the LMC center, the denser the field is.

The $(C-T_1)_o$ color seems to be redder for outer fields when compared to inner ones (Fig. 4*b*). The same happens for clusters but the scatter is much larger. The surface M_{T1} (magnitude obtained from the sum of the individual stars flux per total area observed) for the fields decreases, on average, with the distance from the LMC bar, an expected result (Fig. 4*c*). Although a much more scattered and flat relationship exists for the clusters, in this case a selection effect is in play, since low surface brightness clusters can be seen only far from the LMC bar. Regarding this selection effect, it is interesting to note that ESO 121-SC03 would be very difficult to distinguish if it were at a distance $R \leq 7°$ from the LMC center.

According to Figure 4*d*, the total $(C-T_1)_o$ obtained from the CMD sum of the flux of individual stars has a spread much larger in the clusters [$\Delta(C-T_1)_o \approx 1.5$] than in the fields [$\Delta(C-T_1)_o \approx 0.5$]. This result is consistent with that obtained by Bica et al. (1998); namely, the metallicity range of the intermediate-age LMC clusters is larger than that of their respective fields.

4.2.2. *Density of Field Clump and MS Stars*

Two of the boxes used for building the LFs were employed as representative of the RGC [$-0.35 < M_{T1} < 0.65$ and $0.65 < (C-T_1)_o < 2.0$]. These two boxes enclose the dual clump structure present in the fields of SL 388 and SL 509. The dual clump seen in the CMDs of these fields can be caused by two stellar populations situated at different distances (the fainter clump being the signature of a similar age population or of an older population presenting

TABLE 3

INTEGRATED LIGHT PROPERTIES

Cluster	N (arcmin^{-2})	M_v	M_{T1}	$(C-T_1)_o$
SL 8	53.71	−4.24	−4.83	1.76
Field	24.27	−8.98	−9.43	1.33
SL 126	128.59	−2.78	−3.07	0.85
Field	7.90	−7.32	−7.80	1.48
SL 262	297.93	−3.93	−4.37	1.33
Field	9.46	−7.68	−8.14	1.41
SL 388	254.64	−4.55	−4.95	1.25
Annulus 1	42.02	−6.64	−7.07	1.30
Annulus 2	38.03	−7.17	−7.55	1.15
Annulus 3	33.09	−6.50	−6.86	1.04
Field	35.31	−8.61	−9.02	1.21
IC 2134	151.51	−4.19	−4.39	0.51
Field	27.34	−8.86	−9.26	1.24
SL 451	86.58	−4.08	−4.63	1.66
Field	27.34	−8.86	−9.26	1.24
SL 509	276.29	−4.96	−5.49	1.34
Annulus 1	58.77	−7.11	−7.49	1.11
Annulus 2	56.76	−6.88	−7.32	1.22
Annulus 3	60.24	−6.85	−7.25	1.10
Field	55.72	−8.72	−9.12	1.12
SL 769	258.46	−3.96	−4.26	0.83
Annulus 1	333.57	−7.90	−8.30	1.00
Annulus 2	330.73	−7.95	−8.32	0.93
Annulus 3	326.01	−7.97	−8.32	0.90
Annulus 4	312.28	−8.06	−8.44	0.97
Field	314.72	−9.83	−10.20	0.95
SL 817	189.07	−3.65	−4.03	1.12
Field	55.25	−9.10	−9.51	1.18
ESO 121-SC03	70.54	−5.07	−5.53	1.35
Field	2.71	−7.21	−7.61	1.21
SL 842	113.39	−3.96	−4.56	1.81
Field	8.69	−8.27	−8.75	1.51
SL 862	218.83	−4.45	−4.95	1.43
Field	26.08	−8.97	−9.39	1.28
OHSC 33	134.64	−3.16	−3.45	0.78
Field	21.91	−8.55	−8.96	1.24
OHSC 37	34.37	−3.67	−4.28	2.06
Field	3.07	−8.06	−8.49	1.42

NOTE.—"Field" entries are related to the CCD area minus the area corresponding to twice the cluster radius. "Annulus" entries are related to ring areas corresponding to the radius limits 150 pixels $< r <$ 500 pixels (annulus 1), 500 pixels $< r <$ 691 pixels (2), 691 pixels $< r <$ 840 pixels (3), and 840 pixels $< r <$ 966 pixels (4).

a red horizontal branch) or by an evolutionary effect in a single population. In the former case, the presence of a dwarf galaxy located at the distance of the SMC is a possibility (Bica et al. 1998). Concerning the last case, Girardi et al. (1998) have predicted theoretically the developing of a secondary clump structure in an $M_I \times (V-I)$ diagram of metal-rich populations as a result from the fact that stars slightly heavier than the maximum mass needed to acquire degenerate He cores define a fainter clump 0.3 mag below the red primary clump. Presently, it is premature to apply one of these explanations to our sample. Ideal targets aiming at clarifying such issue are LMC populous fields, for which further observational investigation of the dual clump structure is under way. In the present work the average age of stellar populations is considered, and, therefore, the dual clump structure can introduce some bias in the star counts of the fields surrounding SL 388 and SL 509.

The projected density of stars in the RGC phase for each field was plotted as a function of the deprojected distance R in Figure 5*a*. Figures 5*b*–5*l* show the projected density of stars in 11 segments of the MS. These segments are within the magnitude range $-2.35 < M_{T1} < 3.15$ sampling 0.5 mag bins each. All densities were corrected for Galactic contamination. The drop in the density toward the outer regions of the LMC disk can immediately be noted when one takes any CMD segment and follows it from small to large R in Figure 5. The density of RGC stars increases inward from 8° (≈8 kpc). At larger distances, just a few clump stars are seen for the sampled fields. Indeed, in virtually all diagrams, little or no evidence for a substantial LMC field population is found beyond ∼10°, in good agreement with the results of Bica et al. (1998).

4.2.3. *The Youngest Field Populations*

The fields are a mix of populations of different ages. One can associate different parameters in the CMD of the fields with different ages. The magnitude difference between the most populous turnoff and the RGC is one such parameter to derive an age for the associated population as made by Bica et al. (1998). In the present study an age derived from the brightest field turnoff, revealing the age of the most recent burst of star formation, was determined. It relies on the turnoff R magnitude obtained from $Z = 0.006$ classical isochrones by VandenBerg (1985). Errors were estimated based on the spread in T_1 of the brighter MS stars. Figure 6 shows this age as a function of the density of clump stars (Fig. 6*a*), the density of MS stars within the magnitude range $1.65 < M_{T1} < 2.15$ (Fig. 6*b*), the galactocentric distance (Fig. 6*c*), and the age derived for the richest turnoff (Fig. 6*d*).

Since the fields contain composite populations, it should be recalled that the ages analyzed in the following are averaged ones. There is a clear correlation between the age of the youngest burst and the clump star density: in the range $8 < \log(\text{age}) < 9.5$, the higher the density, the younger the most recent burst (Fig. 6*a*) is. This trend is not as easily discerned for the density of MS stars (Fig. 6*b*), but it is still present. The farther the field from the LMC center, the older its youngest population (Fig. 6*c*) is. The age derived for the youngest field population does not appear to correlate with the age derived from the richest turnoff (Fig. 6*d*). In summary, if these are general results valid throughout the LMC disk, the most recent burst of star formation for a field can be dated from its distance from the LMC center (if it is lower than ≈8 kpc) and/or its density of clump stars.

Inner fields have younger stellar population components than outer ones and, as a consequence, the density of clump stars changes accordingly. Considering that field and cluster populations have similar properties, these results are in agreement with those in Bica et al. (1996), namely, that the younger star clusters and associations are located preferentially in the LMC inner regions while the older clusters are distributed all over the LMC.

4.3. *Ratios of Star Counts as a Function of Astrophysical Parameters*

Bertelli et al. (1992) computed appropriate ratios of star counts for stellar fields in the LMC providing information on the age and intensity of star formation bursts. In the present work the ratio between the number of RGC stars

and the number of MS stars within a given magnitude range was investigated as a function of R, [Fe/H] and age for the fields according to the values computed in Bica et al. (1998). A segment of the MS judged to be the midpoint between the turnoff and the observational limit [$2.15 < M_{T1} < 2.65$ and $-0.35 < (C-T_1)_o < 0.9$] was used. The number of stars in the field CMDs was counted, and the ratio N(RGC)/N(MS) was computed before and after the correction for Galactic contamination. Figure 7 shows the relations of the corrected ratio with astrophysical parameters as well as with the uncorrected ratio, the latter giving an estimate of how the Galactic field foreground stars are affecting the counts in the two boxes used to compute that ratio. In Figure 7*b* this relation is shown, and one can see that the corrected ratio yields lower values than the observed one, which means that contamination is higher on the RGC than on the MS. The point strongly affected by the correction is the field surrounding ESO 121-SC03. Essentially no correlation can be seen between the corrected ratio and R, age, or [Fe/H], unless one considers only the most populous fields (circled squares in Fig. 7*a*). In fact, in these cases there appears to be a tendency toward a correlation with metallicity in the sense that the higher the ratio the lower the metallicity. The deprojected distance is uncorrelated with N(RGC)/N(MS) according to Figure 7*c*. Since the sample spans a narrow range in age (except for ESO 121-SC03), Figure 7*d* evidences a large range of the ratio (0.2–0.55) for a single age. The outer fields surrounding SL 126 and SL 842 are labeled in Figures 7*c* and 7*d*. They present, together with ESO 121-SC03, the oldest average ages of the sampled fields. The very low ratio for ESO 121-SC03 is probably an artifact of small number statistics.

5. SUMMARY AND CONCLUDING REMARKS

With the goal of studying statistically the stellar properties of 14 clusters and surrounding fields in the LMC, boxes were defined in the CMD of these objects. The number of stars within each of these boxes, which sample the main evolutionary sequences (RGB, clump, turnoff), were used to build and compare the luminosity functions of clusters and respective fields. The effect of Galactic star contamination on these luminosity functions was also estimated. In view of large CCD areal coverage (13.′6 × 13.′6) yielding statistically complete CMDs, it was possible to look for LMC stellar-content differences from cluster to respective field and from field to field.

For each field CMD, mean evolutionary sequences were computed based on the mean magnitude and color of the stars within each box. The more populous fields allowed exploration of a possible radial change of the CMD morphology. The CMD structure of the inner populous field around SL 769 allowed us to estimate an integrated color and magnitude and their sensitivity to a changeable small number of bright stars on the giant branch and main sequence. Fluctuations in color and magnitude were found and quantified for the MS turnoff and GB tip. This analysis provides a useful constraint for stellar population studies of composite stellar systems for which only integrated light is available.

Besides CMD morphology, star counts and ratios in well-defined evolutionary sequences were carried out. No correlation was found between the ratio of clump stars to MS stars within a given magnitude range and the distances of the fields from the LMC center. On the other hand, star counts in specific evolutionary phases (RGC and MS) did show a correlation with galactocentric distance reflecting the coupled effect of decreasing density and increasing age toward the outer fields investigated.

Luminosity functions for clusters and fields were presented. Regarding the most populous field LFs, SL 388 and 509 seem to have a shallower main-sequence LF slope than its associated field. Since the observed clusters and fields are located at various distances from the LMC center, reaching as far as $\approx$13 kpc, possible spatial variations of the LMC stellar population were assessed. There is some indication of a $C-T_1$ radial gradient at least from 4° to 8° from the LMC center in the sense that the farther the field the redder it is.

An enlargement of the sample of fields in the LMC at various distances from the bar will certainly clarify correlations that could only be suggested with the present 14 fields, such as the increase of the $C-T_1$ color with increasing distance.

This research is supported in part by NASA through grant GO-06810.01-95A (to D. G.) from the Space Telescope Science Institute, which is operated by the Association of Universities for Research in Astronomy, Inc., under NASA contract NAS5-26555. This work was partially supported by the Brazilian institutions CNPq and FINEP, the Argentine institutions CONICET and CONICOR, and the VITAE and Antorcha foundations. We acknowledge an anonymous referee for interesting remarks.

APPENDIX

ACCOUNTING FOR CROWDING

Renzini (1998) presented a theoretical framework useful for the analysis of CCD photometry whenever individual stars are to be resolved, as is the case in CMD studies. The total luminosity of the stellar population sampled in the CCD frame is related to the number of stars in each evolutionary stage. His study also allows one to see at which magnitude crowding effects become significant, after which the probability of a pixel or resolution element containing a blending of stars is extremely high. At this magnitude level the observed luminosity function would be severely influenced since two or more faint stars would be mistaken as a single brighter star. In order to check the correspondent threshold magnitude, the total bolometric luminosity per pixel was computed for the cluster sample, since the fields are not expected to be affected in a significant way by crowding. The total bolometric luminosity for each cluster was estimated according to

$$L_T = kL_v = k10^{-0.4(M_v - M_{v\odot})}, \quad \text{(A1)}$$

TABLE 4

THRESHOLD T_1 MAGNITUDE FOR CROWDING EVALUATION

Cluster	V	Diaphragm (arcsec)	l_T	T_1 Blue	T_1 Red	T_1 Blue Observed
SL 8.....	14.39	80.00	0.22	25.47	24.70	22.00
	13.80	61.00	0.59	24.40	23.63	
SL 126.....	15.75	60.00	0.10	26.29	25.52	22.50
	...	...	...	...	...	
SL 262.....	14.57	40.00	0.61	24.25	23.48	22.00
	14.25	38.00	0.90	23.82	23.06	
SL 388.....	14.04	60.00	0.51	24.52	23.76	22.50
	13.85	38.00	1.42	23.42	22.66	
IC 2134.....	14.63	60.00	0.44	24.92	24.15	21.80
	13.94	38.00	1.60	23.51	22.74	
SL 451.....	14.74	60.00	0.39	25.03	24.26	21.80
	14.20	38.00	1.26	23.77	23.00	
SL 509.....	13.63	60.00	0.75	24.12	23.35	22.00
	13.23	61.00	0.97	23.83	23.06	
SL 769.....	14.79	60.00	0.34	25.13	24.37	22.80
	13.18	61.00	1.18	23.78	23.01	
SL 817.....	15.07	40.00	0.55	24.56	23.80	21.50
	14.18	38.00	1.18	23.75	22.98	
ESO 121-SC03.....	13.52	160.00	0.12	26.13	25.36	22.60
	14.04	61.00	0.46	24.64	23.87	
SL 842.....	14.63	48.00	0.47	24.63	23.86	21.30
	14.15	38.00	1.08	23.72	22.96	
SL 862.....	14.33	48.00	0.85	24.17	23.40	21.50
	13.67	38.00	1.99	23.24	22.48	
OHSC 33.....	15.62	40.00	0.37	25.06	24.29	21.50
	...	...	...	...	...	
OHSC 37.....	15.31	60.00	0.30	25.47	24.71	22.00
	...	...	...	...	...	

NOTES.—Col. (2): Integrated V magnitude observed by Bica et al. 1996 with the diaphragm used in col. (3). Col. (4): Corresponding bolometric luminosity per pixel (see text for details). Cols. (5), (6), and (7): Threshold magnitudes at which crowding starts to become significant for a blue star $[(C-T_1)_o = 0]$, for a red one $[(C-T_1)_o = 3]$, and for the observed faintest blue stars sampled in the CMDs, respectively.

where $k \sim 1.5$ is the ratio between bolometric and V-band luminosities for intermediate-age populations (Renzini 1998); $M_{v\odot} = 4.82$ is the absolute V magnitude of the sun; and M_v is the integrated absolute V magnitude of the cluster.

In order to compute L_T, a transformation between Washington magnitudes and V from Geisler (1996) was combined with $A(T_1) = 2.62E(B-V)$ and $E(C-T_1) = 1.966E(B-V)$. If $A(V) = 3.12E(B-V)$ is adopted, the following relation results:

$$M_v = 0.052 + 0.256(C-T_1)_o + M_{T1} + 0.0017E(C-T_1)\,, \tag{A2}$$

where $(C-T_1)_o$ and M_{T1} are the integrated color and magnitude of the clusters that can be obtained directly from the observed CMDs. Since the last term in equation (A2) is negligible, L_T results:

$$L_T = k10^{-0.4[0.052+0.256(C-T_1)_o+M_{T1}-M_{v\odot}]}\,. \tag{A3}$$

Then the total bolometric luminosity per pixel is given by

$$l_T = L_T/N_{\rm pix}\,, \tag{A4}$$

where $N_{\rm pix}$ corresponds to the sampled area in pixels.

In this way, we obtain the total light per pixel, which is to be compared with the light of a single star. Relatively small magnitude errors can be obtained only for stars brighter than l_T. For example, if the magnitude corresponding to l_T is faint, only stars that are even brighter should be considered in a CMD analysis. Then, the threshold apparent magnitude at which crowding becomes important is derived from equation (A4) by substituting L_T from equation (A3), i.e.,

$$T_1 = M_{v\odot} - 0.052 + (T_1 - M_{T1}) - 0.256[(C-T_1) - E(C-T_1)] - 2.5\log\frac{l_T}{k}\,, \tag{A5}$$

where every quantity refers to a pixel.

In practice two different observables were employed to get L_T: (1) the cluster photoelectric integrated V magnitude (Bica et al. 1996) through equation (A1) and (2) the number of stars used to build the CMD through equation (A3). In order to compute $N_{\rm pix}$ in the former case, an equivalent number of pixels was determined from the area observed through the

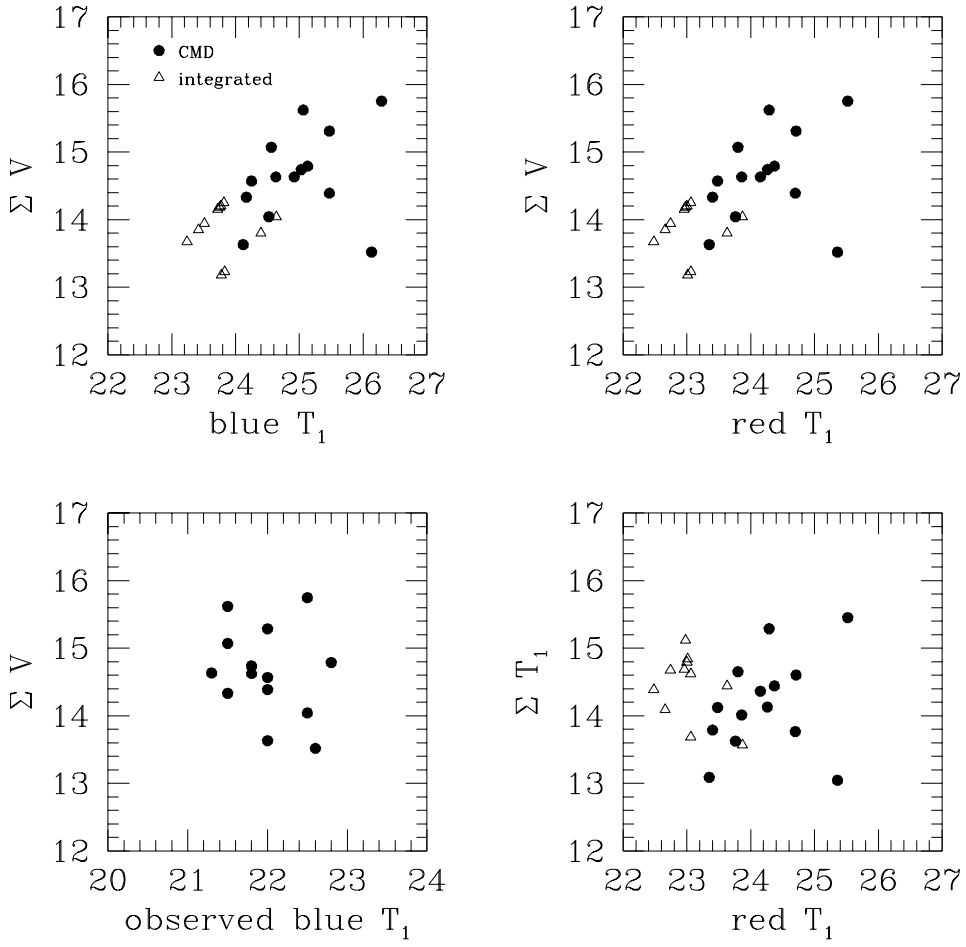

FIG. 8.—Total cluster apparent magnitudes obtained from observed integrated photometry (*triangles*) and from addition of CMD star fluxes (*filled circles*) as a function of the threshold magnitude, fainter than which crowding prevents good photometry. ΣT_1 is the total cluster apparent magnitude in the T_1-band and ΣV in the V-band. Red and blue T_1 correspond to the threshold magnitude, as computed from eq. (A5) and listed in Table 4, for a $C-T_1=3$ star and a $C-T_1=0$ star, respectively. Observed blue T_1 is the threshold magnitude measured for a blue star in the cluster CMDs. No cluster observed integrated photometry is shown in the lower left panel in order to see more clearly how the CMD total flux behaves with an observed threshold magnitude.

diaphragm using the same scale as the CCD observations. These two approaches give different results since CMDs require individual stars to be selected on the basis of a well-defined point spread function and crowding affects it, therefore preventing a complete sampling of the observed cluster stars. On the other hand, integrated light measurements are not affected by crowding. As a consequence, the total V flux computed from the number of stars in the CMDs is smaller than the one computed from the integrated V magnitude if the observed area is the same.

Table 4 shows the results for the cluster sample. Since the threshold T_1 magnitude depends on $C-T_1$, it was computed for a red star ($C-T_1=3$) and a blue one ($C-T_1=0$) from equation (A5). The fact that all clusters present threshold T_1 fainter than that for the dimmest stars observed in the CMDs demonstrates that the selection criteria used to get good quality photometry already discarded stars in crowded regions. Figure 8 presents cluster total apparent magnitudes (V or T_1) from integrated photometry (*open triangles*) and addition of CMD stars flux (*filled circles*) as a function of the threshold magnitude for red stars and blue ones. ΣT_1 is the total cluster apparent magnitude in the T_1-band and ΣV in the V-band. Observed blue T_1 is the fainter magnitude measured for a blue star in the cluster CMDs. In order to compare exclusively CMD based properties the lower left panel does not show cluster total apparent magnitudes from integrated photometry. The upper panels show that the brighter the cluster, the brighter the threshold magnitude is, this trend being more evident for the total V from integrated light. No correlation was found between the CMD V flux and the observed threshold for blue stars in our CMD sample, as one can see in the lower left panel. In general, integrated photometry gives brighter V fluxes than CMD sums, as expected.

REFERENCES

Bahcall, J. N., & Soneira, R. M. 1980, ApJS, 44, 73
Bertelli, G., Mateo, M., Chiosi, C., & Bressan, A. 1992, ApJ, 388, 400
Bica, E., Clariá, J. J., Dottori, H., Santos, J. F. C., Jr., & Piatti, A. E. 1996, ApJS, 102, 57
Bica, E., Geisler, D., Dottori, H., Clariá, J. J., Piatti, A. E., & Santos, J. F. C., Jr. 1998, AJ, 116, 723
Butcher, H. 1977, ApJ, 216, 327
Canterna, R. 1976, AJ, 71, 228
Corsi, C. E., Buonanno, R., Fusi Pecci, F., Ferraro, F. R., Testa, V., & Greggio, L. 1994, MNRAS, 271, 385
Elson, R. A. W., Gilmore, G. F., & Santiago, B. X. 1997, MNRAS, 289, 157
Ferraro, F. R., Fusi Pecci, F., Testa, V., Greggio, L., Corsi, C. E., Buonanno, R., Terndrup, D. M., & Zinnecker, H. 1995, MNRAS, 272, 391
Geha, M., et al. 1998, AJ, 115, 1045

Geisler, D. 1996, AJ, 111, 480
Geisler, D., Bica, E., Dottori, H., Clariá, J. J., Piatti, A. E., & Santos, J. F. C., Jr. 1997, AJ, 114, 1920
Girardi, L., Groenewegen, M. A. T., Weiss, A., & Salaris, M. 1998, MNRAS, 301, 149
Hardy, E., Buonanno, R., Corsi, C. E., Janes, K. A., & Schommer, R. A. 1984, ApJ, 278, 592
Hodge, P. W. 1987, PASP, 99, 730
Lauberts, A. 1982, The ESO/Uppsala Survey of the ESO (B) Atlas (Munich: ESO)
Lyngå, G., & Westerlund, B. E. 1963, MNRAS, 127, 31
Olszewski, E. W., Harris, H. C., Schommer, R. A., & Canterna, R. W. 1988, AJ, 95, 84
Olszewski, E. W., Suntzeff, N. B., & Mateo, M. 1996, ARA&A, 34, 511
Ratnatunga, K. U., & Bahcall, J. N. 1985, ApJS, 59, 63
Renzini, A. 1998, AJ, 115, 2459
Sarajedini, A. 1998, AJ, 116, 738
Shapley, H., & Lindsay, E. M. 1963, Irish Astron. J., 6, 74
Stetson, P. B. 1987, PASP, 99, 191
Stryker, L. L. 1984, ApJS, 55, 127
Vallenari, A., Chiosi, C., Bertelli, G., & Ortolani, S. 1996, A&A, 309, 358
VandenBerg, D. A. 1985, ApJS, 58, 711
Westerlund, B. E., Linde, P., & Lyngå, G. 1995, A&A, 298, 39